

Article

The Structure and Microwave Dielectric Properties of $\text{MgTi}_{1-x}(\text{Mn}_{1/3}\text{Nb}_{2/3})_x\text{O}_3$ Ceramics

Huan Huang , Baoyang Li, Fanshuo Wang, Yuanming Lai * and Gang Jiang *

School of Mechanical and Electrical Engineering, Chengdu University of Technology, Chengdu 610059, China

* Correspondence: laiyuanming19@cdut.edu.cn (Y.L.); jianggang@cdut.edu.cn (G.J.)

Abstract: $\text{MgTi}_{1-x}(\text{Mn}_{1/3}\text{Nb}_{2/3})_x\text{O}_3$ ($x = 0\text{--}0.30$) ceramics were prepared via the solid-state reaction method. The phase composition, microstructure, bond characteristics, and microwave dielectric properties of $\text{MgTi}_{1-x}(\text{Mn}_{1/3}\text{Nb}_{2/3})_x\text{O}_3$ ($x = 0\text{--}0.30$) were systematically investigated. The $\text{MgTi}_{1-x}(\text{Mn}_{1/3}\text{Nb}_{2/3})_x\text{O}_3$ ceramics presented an ilmenite type with an $R\text{-}3$ space group, and the secondary-phase MgTi_2O_5 only existed at $x = 0$ and 0.30 . The introduction of $(\text{Mn}_{1/3}\text{Nb}_{2/3})^{4+}$ effectively suppressed the formation of the MgTi_2O_5 phase. The variation trend of the dielectric constant (ϵ_r) was the same as relative density. The quality factor (Q_f) value was enhanced by the stable microstructure, which was caused via the lattice energy of $\text{Ti}/(\text{Mn}_{1/3}\text{Nb}_{2/3})\text{-O}$ bonds. And a high Q_f value (353,000 GHz) was obtained for $\text{MgTi}_{1-x}(\text{Mn}_{1/3}\text{Nb}_{2/3})_x\text{O}_3$ ($x = 0.04$) ceramics sintered at 1250°C . In addition, the introduction of Mn^{2+} ions with a larger ionic radius exacerbates the distortion of TiO_6 octahedra, leading to significant fluctuations in the temperature coefficient of the resonance frequency (τ_f) value.

Keywords: MgTiO_3 ceramic co-substitution; microwave dielectric properties; lattice energy; octahedral distortion



Citation: Huang, H.; Li, B.; Wang, F.; Lai, Y.; Jiang, G. The Structure and Microwave Dielectric Properties of $\text{MgTi}_{1-x}(\text{Mn}_{1/3}\text{Nb}_{2/3})_x\text{O}_3$ Ceramics. *Crystals* **2023**, *13*, 1050. <https://doi.org/10.3390/cryst13071050>

Academic Editors: Wen Lei and Kaixin Song

Received: 1 June 2023

Revised: 21 June 2023

Accepted: 27 June 2023

Published: 2 July 2023



Copyright: © 2023 by the authors. Licensee MDPI, Basel, Switzerland. This article is an open access article distributed under the terms and conditions of the Creative Commons Attribution (CC BY) license (<https://creativecommons.org/licenses/by/4.0/>).

1. Introduction

As 5G communication technology gradually shifts towards the millimeter wave band, the trend towards higher frequencies has further raised the performance requirements for microwave devices. There is an increasing demand for the miniaturization, integration, and lightweight design of microwave circuits. Compared to traditional metallic cavity resonators, dielectric resonators possess advantages such as miniaturization, low cost, high reliability, and high stability. The microwave dielectric performance of materials plays a crucial role in determining their overall performance. To meet this requirement, it is generally necessary to have a moderate dielectric constant (ϵ_r), high quality factor (Q_f), and near-zero temperature coefficient of resonance frequency (τ_f).

MgTiO_3 is an ABO_3 ilmenite-type structure, which has garnered considerable attention from numerous researchers due to its relatively high Q_f value ($Q_f \sim 160,000$ GHz). In general, the microwave dielectric properties of MgTiO_3 are affected by intrinsic structural characteristics such as bond characteristics and octahedron distortion [1]. These characteristics can be modified by varying cations at Mg or Ti sites. Researchers have investigated the variations in the Q_f value caused by the addition of 36 different dopants in TiO_2 ceramics [2]. It was found that significant improvements in the Q_f value occur when the Ti site is substituted with low-valence cations. However, the introduction of low-valence cations solely for Ti substitution may lead to lattice defects. Therefore, to improve the microwave dielectric properties of MgTiO_3 ceramics, the intrinsic structural characteristics were tailored via the substitution of the Ti site [3–11]. The substitution of the Ti site in a MgTiO_3 ceramic with $(\text{Mn}_{1/2}\text{W}_{1/2})^{4+}$ reveals that the presence of Mn^{2+} eliminates the detrimental effect of Ti^{3+} on the Q_f value of the ceramic and suppresses the formation of the secondary-phase MgTi_2O_5 . However, the continuous introduction of Mn^{2+} and W^{6+} ions, while suppressing Ti^{3+} , does

not significantly enhance the Q_f value compared to pure MgTiO_3 ceramics. In addition, we have found that $(\text{Zn}_{1/3}\text{Nb}_{2/3})^{4+}$ can enhance the microwave dielectric properties, especially the Q_f value, and lower the sintering temperature of MgTiO_3 ceramics [12]. And the τ_f value was related to the structural distortion. Meanwhile, in previous works, there are some relationships between ionic radii and the structure distortion, which relates to the microwave dielectric properties. Furthermore, the existence of Nb^{5+} could suppress Ti^{4+} to Ti^{3+} and therefore enhance the Q_f value [5]. Hence, based on the inhibition of Ti^{4+} reducibility by Nb^{5+} and Mn^{2+} ions and their larger ionic radii, the $(\text{Mn}_{1/3}\text{Nb}_{2/3})^{4+}$ were considered as an alternative ion to improve the microwave dielectric properties of MgTiO_3 . In the present work, $\text{MgTi}_{1-x}(\text{Mn}_{1/3}\text{Nb}_{2/3})_x\text{O}_3$ ($x = 0-0.30$) ceramics were synthesized via solid-state reactions, and their phase composition, microstructure, bond characteristics, and microwave dielectric properties were investigated. Furthermore, the correlations among them were analyzed and established in detail.

2. Experimental Procedures

High-purity MgO , TiO_2 , MnCO_3 , and Nb_2O_5 powders were employed as the raw materials to synthesize the $\text{MgTi}_{1-x}(\text{Mn}_{1/3}\text{Nb}_{2/3})_x\text{O}_3$ ($x = 0, 0.04, 0.12, 0.20$ and 0.30) ceramics via the solid state reaction. The raw material was weighed according to the stoichiometric ratio. Next, the mixed powder was placed into the ball milling jar and milled for 4 h. The slurry was dried. Subsequently, the mixed powder was calcined at $1100\text{ }^\circ\text{C}$ for 4 h. After calcination, the powder was ball-milled to break the agglomerates and dried again. Subsequently, the powder was mixed with PVA (10 wt%) and pressed into pellets under the pressure of 20 MPa. These pellets were 12 mm in diameter and 6–7 mm in thickness. The pressed disks were pre-heated at $600\text{ }^\circ\text{C}$ for 4 h to evaporate PVA and then sintered at $1250-1350\text{ }^\circ\text{C}$ for 4 h. The $x = 0$ sample served as a control sample.

An X-ray diffractometer (XRD) is used to determine the phase composition and crystal structure of a sample under the conditions of $\text{Cu-K}\alpha$ radiation and a scanning range of 10° to 120° . Scanning electron microscopy (SEM) is used to observe the microscopic morphology of ceramic surfaces and is usually shared with Energy Dispersive Spectroscopy (EDS) to analyze the elemental composition and content of the sample surface. The bulk density (ρ_{bulk}) is measured using Archimedes' drainage method. Here, the microwave dielectric properties of the ceramic samples were measured based on the Hakki–Coleman method, and the τ_f values were calculated from the resonance frequencies at $25\text{ }^\circ\text{C}$ and $85\text{ }^\circ\text{C}$:

$$\tau_f = \frac{f(85\text{ }^\circ\text{C}) - f(25\text{ }^\circ\text{C})}{60 \times f(25\text{ }^\circ\text{C})} \times 10^6 \quad (1)$$

3. Results and Discussion

3.1. Phase Composition and Structure Analysis

Figure 1a shows the XRD patterns of the $\text{MgTi}_{1-x}(\text{Mn}_{1/3}\text{Nb}_{2/3})_x\text{O}_3$ ($x = 0-0.30$) ceramics obtained via sintering at $1250\text{ }^\circ\text{C}$. It can be observed that the major phase of MgTiO_3 ($R-3$, PDF #06-0494) was present in all samples, while the secondary-phase MgTi_2O_5 (PDF #76-2373) appeared only at $x = 0$ and 0.30 [13]. The results indicated that appropriate amounts of Mn^{2+} and Nb^{5+} ions could effectively suppress the formation of the MgTi_2O_5 phase. Figure 1b shows the crystal structure of MgTiO_3 , from which it can be seen that this structure consists of two kinds of octahedra, MgO_6 and TiO_6 , which are arranged alternately in the order of $\text{Mg-Ti-Mg-Ti-}\dots$ in the z -axis direction.

In order to further analyze the crystal structure of samples, the XRD patterns of the $\text{MgTi}_{1-x}(\text{Mn}_{1/3}\text{Nb}_{2/3})_x\text{O}_3$ ($x = 0-0.30$) ceramics were refined by FullProf software (FullProf 2020.6) [14], and the refinement results are plotted in Figure 2. The refinement curves and XRD patterns agreed well, indicating that the refinement results are reliable. The structural parameters are listed in Table 1. The cell parameters (a , b , c) and cell volume (V) kept increasing with increasing x . The main contribution to the ionic radius of $(\text{Mn}_{1/3}\text{Nb}_{2/3})^{4+}$ (0.703 \AA), which was larger than that of Ti (0.605 \AA), entered into the lattice and resulted

in the expansion of the lattice [9,15]. By further observation, it was found that the bond lengths showed irregular variations. There was a correlation between these chemical bond changes and microwave dielectrics [16,17].

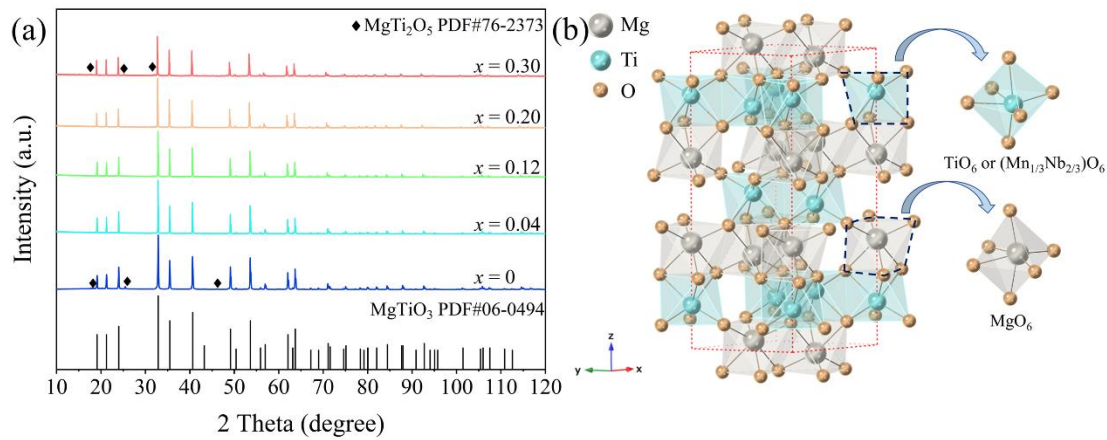


Figure 1. Phase composition and crystal structure of $\text{MgTi}_{1-x}(\text{Mn}_{1/3}\text{Nb}_{2/3})_x\text{O}_3$ ($x = 0\text{--}0.30$) ceramics sintered at $1250\text{ }^\circ\text{C}$: (a) XRD patterns; (b) crystal structure.

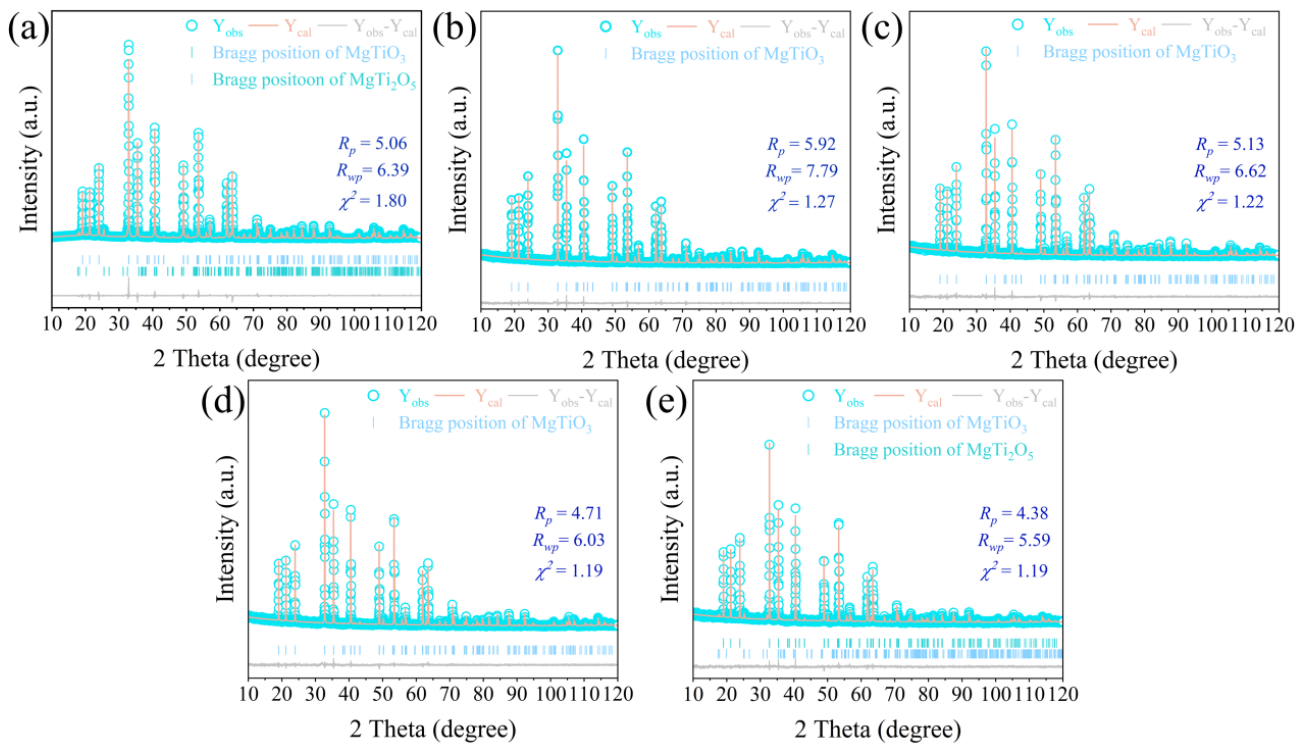


Figure 2. Rietveld refinement of $\text{MgTi}_{1-x}(\text{Mn}_{1/3}\text{Nb}_{2/3})_x\text{O}_3$ ($x = 0\text{--}0.30$) ceramics sintered at $1250\text{ }^\circ\text{C}$: (a) $x = 0$; (b) $x = 0.04$; (c) $x = 0.12$; (d) $x = 0.20$; (e) $x = 0.30$.

3.2. Micromorphology

Figure 3 shows the microscopic morphology of $\text{MgTi}_{1-x}(\text{Mn}_{1/3}\text{Nb}_{2/3})_x\text{O}_3$ ceramics sintered at different temperatures. In comparison to the $x = 0$ sample (refer to Supplementary Figure S1), a discernible trend was observed where the grain size progressively increased and the number of pores gradually diminished with the increasing value of x . This indicated that the incorporation of Mn^{2+} and Nb^{5+} ions imparted a denser structure to the ceramics while simultaneously resulting in the formation of delicate specks on the surface of the samples. Upon further observation, the grain size gradually increased with the increase in temperature at the same x . Abnormal grain growth occurred at $1350\text{ }^\circ\text{C}$,

indicating that the temperature had a promoting effect on the grain growth. It also demonstrated that the introduction of Mn^{2+} and Nb^{5+} ions could reduce the sintering temperature of the system and improve the sintering behaviors of the ceramics.

Table 1. Lattice parameters of $\text{MgTi}_{1-x}(\text{Mn}_{1/3}\text{Nb}_{2/3})_x\text{O}_3$ ($x = 0-0.30$) ceramics at 1250 °C.

x	0	0.04	0.12	0.20	0.30
a (Å)	5.059	5.060	5.067	5.071	5.074
b (Å)	5.059	5.060	5.067	5.071	5.074
c (Å)	13.910	13.915	13.941	13.961	13.991
V (Å ³)	308.31	308.55	309.98	310.86	312.00
W_{f1} (%)	95.75	100	100	100	91.88
W_{f2} (%)	4.25	/	/	/	8.12
Mg-O(1) ¹ (Å)	2.034	2.055	2.050	2.031	2.058
Mg-O(1) ² (Å)	2.175	2.167	2.175	2.171	2.170
Ti/(Mn _{1/3} Nb _{2/3})-O(1) ¹ (Å)	1.878	1.868	1.875	1.891	1.884
Ti/(Mn _{1/3} Nb _{2/3})-O(1) ² (Å)	2.093	2.089	2.092	2.110	2.093

W_{f1} : weight fraction of MgTiO_3 phase; W_{f2} : weight fraction of MgTi_2O_5 phase. ^{1, 2} represent two distinct types of chemical bonds that are exported using the FullProf software.

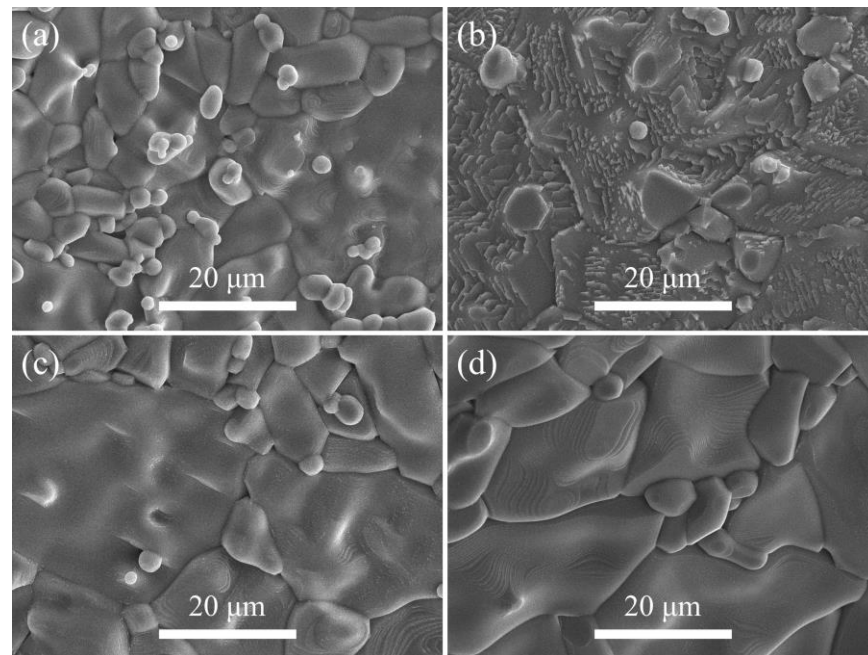


Figure 3. The SEM images of $\text{MgTi}_{1-x}(\text{Mn}_{1/3}\text{Nb}_{2/3})_x\text{O}_3$ ceramics: (a) $x = 0.04$, 1250 °C; (b) $x = 0.12$, 1250 °C; (c) $x = 0.04$, 1300 °C; (d) $x = 0.04$, 1350 °C.

In order to analyze the elemental species and content of the ceramic surface, EDS analysis was performed on the surface of $\text{MgTi}_{0.96}(\text{Mn}_{1/3}\text{Nb}_{2/3})_{0.04}\text{O}_3$ ceramics sintered at 1250 °C. The test areas of the ceramic surface and the elemental composition of each test area are marked in Figure 4, from which it can be seen that both areas contained only Mg, Ti, Mn, Nb and O elements, and $\text{Mg}:(\text{Ti}, \text{Mn}, \text{and Nb}) = 1:1$, which also confirms the XRD analysis results that Mn and Nb ions enter into the lattice and form a solid solution.

3.3. Microwave Dielectric Properties

Figure 5 illustrates the trends of the ϵ_r values of $\text{MgTi}_{1-x}(\text{Mn}_{1/3}\text{Nb}_{2/3})_x\text{O}_3$ ceramics at 1250 °C, along with the associated influencing factors. A variation in ϵ_r is typically closely intertwined with factors such as relative density, the presence of a second phase, and the total distortion [18,19]. When examining the impact of relative density on the ϵ_r value of ceramics, it is often crucial to account for the influence of porosity. To address this, a

correction was applied to the ϵ_r value, yielding the corrected dielectric constant (ϵ_c), using the following equation [20]:

$$P = 1 - \rho_r \tag{2}$$

$$\epsilon_c = \epsilon_r(1 + 1.5P) \tag{3}$$

where P is the porosity and ρ_r is the relative density.

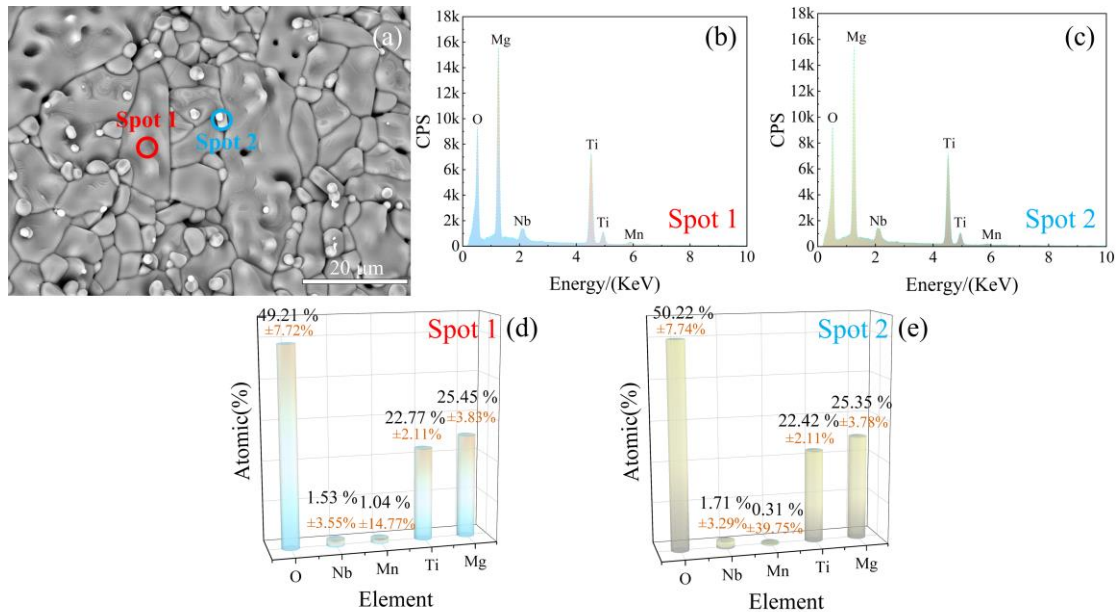


Figure 4. EDS results of $\text{MgTi}_{0.96}(\text{Mn}_{1/3}\text{Nb}_{2/3})_{0.04}\text{O}_3$ ceramics at 1250 °C: (a) EDS test regions; (b) elemental composition of Spot 1; (c) elemental composition of Spot 2; (d) elemental percentage of Spot 1; (e) elemental percentage of Spot 2.

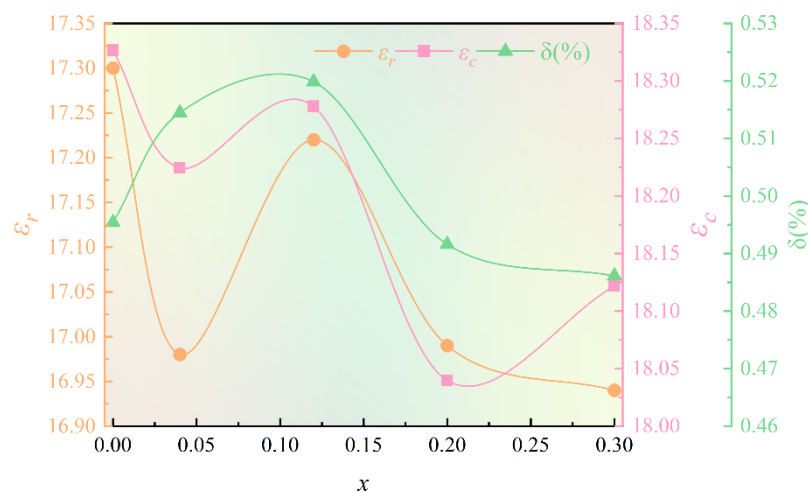


Figure 5. The impact of total distortion and porosity on the ϵ_r values of $\text{MgTi}_{1-x}(\text{Mn}_{1/3}\text{Nb}_{2/3})_x\text{O}_3$ ($x = 0\text{--}0.30$) ceramics, sintered at 1250 °C, was investigated.

Through a careful analysis of Figure 5, it becomes evident that both the actual dielectric constant (ϵ_r) and the corrected dielectric constant (ϵ_c) exhibited an inverse trend compared to the total distortion within the phase range from $x = 0$ to $x = 0.04$. Notably, this observation can be attributed to the presence of a second phase, MgTi_2O_5 , at $x = 0$, which displayed a dielectric constant of $\epsilon_r = 17.4$, while MgTiO_3 exhibited $\epsilon_r = 17$ [21,22]. Therefore, we can infer that the influence of the second phase during this range was responsible for

this phenomenon. In order to investigate the impact of the second phase (MgTi_2O_5) on the ϵ_r value of $\text{MgTi}_{1-x}(\text{Mn}_{1/3}\text{Nb}_{2/3})_x\text{O}_3$ ceramics, we employed a mixed law equation to calculate the theoretical permittivity (ϵ_{theo}) of the ceramics. The equation utilized is as follows [23]:

$$\ln \epsilon_{theo} = V_1 \ln \epsilon_{theo1} + V_2 \ln \epsilon_{theo2} \quad (4)$$

where V_1 , V_2 , ϵ_{theo1} , and ϵ_{theo2} denote the volume fraction and theoretical dielectric constant of each phase.

In the depicted range from $x = 0.04$ to $x = 0.3$, as observed in Figure 5, we observed remarkable alignment between the actual dielectric constant (ϵ_r) and the total distortion (δ). This alignment strongly suggests that the total distortion (δ) exerted the most dominant influence on the ϵ_r value within this interval. This phenomenon can be attributed to the direct relationship between an increase in total distortion and a subsequent rise in the ion polarization rate, ultimately resulting in a larger dielectric constant (ϵ_r) value. Conversely, a decrease in total distortion led to a lower ion polarization rate, consequently resulting in a smaller ϵ_r value. The total distortion of MgO_6 and TiO_6 could be quantified by employing the following equation [23]:

$$\delta = \frac{1}{6} \sum \left(\frac{R_i - \bar{R}}{\bar{R}} \right)^2 \quad (5)$$

An intriguing observation arises from the analysis of Figure 5, where a distinct inverse relationship emerged between the actual dielectric constant (ϵ_r) and the modified dielectric constant (ϵ_c) within the interval ranging from $x = 0.2$ to $x = 0.3$. The underlying disparity could likely be attributed to the influence of porosity on the relative density of the ceramics, consequently impacting the variability in ϵ_r values. Moreover, it is worth highlighting the close correspondence between the fluctuation in ϵ_r values within this range and the variation in total distortion (δ). This suggests that the changes in ϵ_r values during this specific interval were governed by both δ and porosity. Although the presence of a secondary phase did contribute to the alteration in ϵ_r values, its influence appeared to be of secondary significance.

Figure 6a demonstrates the trend of Q_f values of $\text{MgTi}_{1-x}(\text{Mn}_{1/3}\text{Nb}_{2/3})_x\text{O}_3$ ($x = 0-0.30$) ceramics sintered at different temperatures, and it can be seen from the figure that the sample presented the highest Q_f at $x = 0.04$ and a sintering temperature of 1250°C . In addition, Q_f showed a decreasing trend when the x value or the temperature increased, which indicates that Mn and Nb ions were introduced to lower the sintering temperature of the system and also increase the Q_f of the system. To further analyze the factors affecting the Q_f in this experiment, the Q_f of $\text{MgTi}_{0.96}(\text{Mn}_{1/3}\text{Nb}_{2/3})_{0.04}\text{O}_3$ ceramics obtained via sintering at 1250°C was investigated to explore the influencing factors.

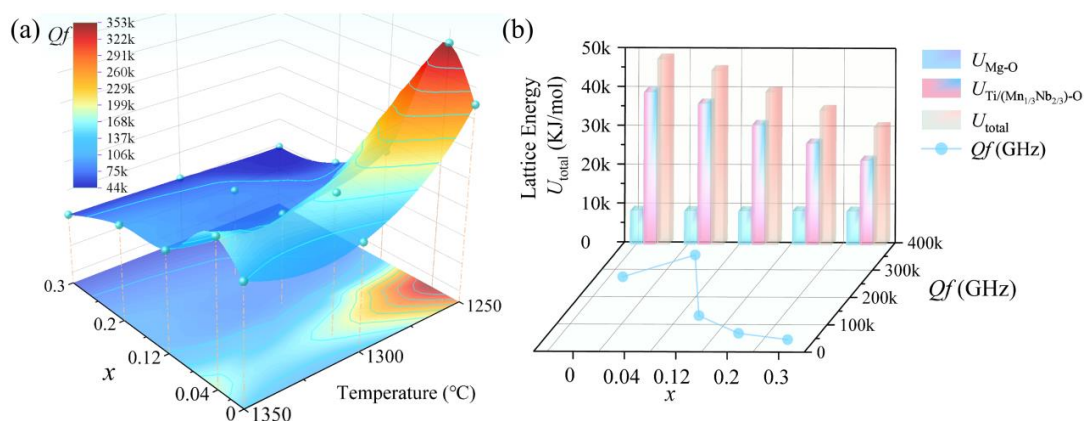


Figure 6. The variation in Q_f value for $\text{MgTi}_{1-x}(\text{Mn}_{1/3}\text{Nb}_{2/3})_x\text{O}_3$ ($x = 0-0.30$) ceramics. (a) The effect of different sintering temperatures on Q_f ; (b) the relationships between Q_f and lattice energy at 1250°C .

There have been numerous studies that have delved into the factors influencing microwave dielectric properties [24–27]. In general, Qf is mainly affected by both intrinsic and non-intrinsic factors. Both intrinsic and extrinsic factors contribute to the total loss of a material, where intrinsic losses primarily depend on the crystal structure, while extrinsic losses arise from second phases, crystal defects, and porosity, among others [8,9,11,28]. In this section, the impact of chemical bond properties on crystal structure and microwave dielectric properties is investigated using the complex chemical bond theory.

According to the complex chemical bond theory, each compound crystal can be decomposed into a superposition of several binary crystal sub-formulas (A_mB_n), where A and B represent different types of cations and anions, respectively [17]. Thus, $MgTi_{1-x}(Mn_{1/3}Nb_{2/3})_xO_3$ ($x = 0-0.30$) can be decomposed into the following binary crystal sub-formulas:

$$MgTi_{1-x}(Mn_{1/3}Nb_{2/3})_xO_3 = Mg_{1/2}O(1)_{3/4}^1 + Mg_{1/2}O(1)_{3/4}^2 + Ti_{1-x/2}O(1)_{3-3x/4}^1 + Ti_{1-x/2}O(1)_{3-3x/4}^2 + (Mn_{1/3}Nb_{2/3})_{x/2}O(1)_{3x/4}^1 + (Mn_{1/3}Nb_{2/3})_{x/2}O(1)_{3x/4}^2 \quad (6)$$

In general, lattice energy is defined as the energy required to separate one mole of a crystal into gaseous free ions, reflecting the vibrational energy of ions and the stability of chemical bonds within the crystal [29]. Higher lattice energy (U) results in lower internal losses caused by lattice polarization under an electric field, leading to a higher Qf [30]. For this purpose, we calculated the lattice energy equation based on Equations (7)–(10).

$$U_{cal} = \sum_{\mu} U_b^{\mu} \quad (7)$$

$$U_b^{\mu} = U_{bc}^{\mu} + U_{bi}^{\mu} \quad (8)$$

$$U_{bc}^{\mu} = 2100m \frac{(Z_+^{\mu})^{1.64}}{(d^{\mu})^{0.75}} f_c^{\mu} \quad (9)$$

$$U_{bi}^{\mu} = 1270 \frac{(m+n)Z_+^{\mu}Z_-^{\mu}}{d^{\mu}} \left(1 - \frac{0.4}{d^{\mu}}\right) f_i^{\mu} \quad (10)$$

The Qf value variations in $MgTi_{0.96}(Mn_{1/3}Nb_{2/3})_{0.04}O_3$ ceramics obtained via sintering at 1250 °C are presented in Figure 6b. Meanwhile, the lattice energy and total lattice energy of the Mg-O bond and Ti/($Mn_{1/3}Nb_{2/3}$)-O bond in each component are plotted in Figure 6b. It can be observed that the lattice energy of the Mg-O bond showed minimal variation, whereas the lattice energy of the Ti/($Mn_{1/3}Nb_{2/3}$)-O bond and the overall total lattice energy decreased with increasing x . In addition, the lattice energy of the Ti/($Mn_{1/3}Nb_{2/3}$)-O bond was higher compared with that of the Mg-O bond, indicating that the Ti/($Mn_{1/3}Nb_{2/3}$)-O bond made a significant contribution to the total lattice energy and had more influence on the Qf when sintered at 1250 °C [17]. The sample with $x = 0.04$ had the highest Qf value; however, the corresponding total lattice energy was lower at this time compared to the sample with $x = 0$. In general, the higher the lattice energy, the higher the Qf , but the Qf of the sample with $x = 0$ was lower than that of the sample with $x = 0.04$ due to the presence of the second-phase $MgTi_2O_5$ ($Qf = 47,000$ GHz) in the sample with $x = 0$ [17,31]. At $x > 0.04$, the trends of lattice energy and Qf were in agreement, indicating that lattice energy and the second phase are the main factors that affected Qf in this experiment.

τ_f is an essential consideration in the practicality of microwave dielectric ceramics, which represents the temperature stability of microwave components in the operating environment. According to Equation (11), the variation in τ_f is closely related to the

dielectric constant temperature coefficient (τ_ϵ), and Equation (12) is the expression for τ_ϵ obtained by differentiating the Clausius–Mossotti equation [32,33].

$$\tau_f = -\left(\frac{\tau_\epsilon}{2} + \alpha_L\right) \quad (11)$$

$$\begin{aligned} \tau_\epsilon &= \frac{(\epsilon-1)(\epsilon+2)}{\epsilon} \left[\frac{1}{\alpha_D} \left(\frac{\partial \alpha_D}{\partial T} \right)_V + \frac{1}{\alpha_D} \left(\frac{\partial \alpha_D}{\partial V} \right)_T \left(\frac{\partial V}{\partial T} \right)_P - \frac{1}{V} \left(\frac{\partial V}{\partial T} \right)_P \right] \\ &= \frac{(\epsilon-1)(\epsilon+2)}{\epsilon} (A + B + C) \end{aligned} \quad (12)$$

where α_L is considered as a constant, 10 ppm/°C. α_D and V represent the polarizability of the sample and the volume of a small sphere. Part A is a dependence of polarizability on temperature; Part B represents an increase in the polarizability of a constant number of particles with the increment in the available volume while the temperature increases; Part C presents the decrease in the number of polarizable particles per unit volume while the temperature increases [34]. Since the Parts B and C have similar magnitudes and opposite signs, τ_ϵ is generally determined by Part A . In addition, Part A is related to the restoring force of chemical bonds, which is in turn correlated with the degree of structural distortion [33]. And this structural alteration will have an impact on τ_f . In this section, we analyze the effect of TiO_6 octahedral distortion (Δ_{Ti}) on τ_f . Therefore, we calculate Δ_{Ti} in the system using Equation (13) and judge the magnitude of the bond-restoring force in its different states according to the degree of distortion of the TiO_6 octahedra, which is related to the polarizability and thus affects the value of τ_ϵ , which is finally reflected in τ_f .

$$\Delta_{Ti} = \frac{1}{6} \times \sum \left(\frac{R_i - R_{ave}}{R_{ave}} \right)^2 \quad (13)$$

Figure 7 plots the trends of τ_f and Δ_{Ti} for $\text{MgTi}_{1-x}(\text{Mn}_{1/3}\text{Nb}_{2/3})_x\text{O}_3$ ($x = 0-0.30$) ceramics sintered at 1250 °C. From Figure 7, it can be observed that the trends of τ_f and Δ_{Ti} were opposite, with a decrease in distortion indicating an increase in recovery. Recovery is inversely proportional to polarization capacity. Therefore, an increase in recovery leads to a decrease in polarization capacity, resulting in a decrease in the value of Part A . This decrease in Part A also causes a decrease in τ_f , thereby affecting its value and causing it to shift in the positive direction.

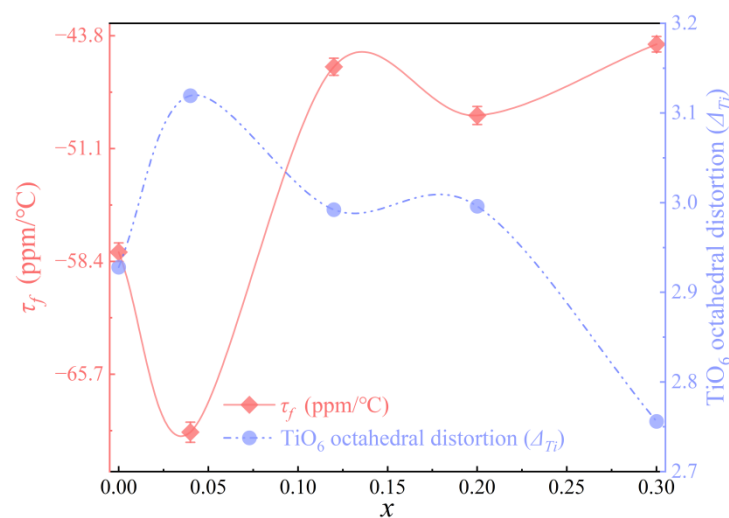


Figure 7. Relationships of τ_f and TiO_6 distortion (Δ_{Ti}) for $\text{MgTi}_{1-x}(\text{Mn}_{1/3}\text{Nb}_{2/3})_x\text{O}_3$ ($x = 0-0.30$) ceramics sintered at 1250 °C.

Figure 8 provides a comparative analysis of various MgTiO_3 -based ceramics [3–10,12,35]. However, in the case of most ion-substituted MgTiO_3 ceramics, achieving high Q_f values

typically requires modifications to the structure of the oxygen octahedra. In our study, we successfully adjusted the structure of TiO_6 octahedra by introducing $(\text{Mn}_{1/3}\text{Nb}_{2/3})^{4+}$ substitutions. This resulted in significantly higher Qf values and improved τ_f values, all while using lower sintering temperatures. Notably, the $\text{MgTi}_{1-x}(\text{Mn}_{1/3}\text{Nb}_{2/3})_x\text{O}_3$ ceramics with $x = 0.04$, sintered at 1250°C , exhibited the most exceptional performance. These findings indicate that by precisely adjusting the crystal structure, it becomes possible to modify the microwave dielectric properties, offering promising prospects for practical applications.

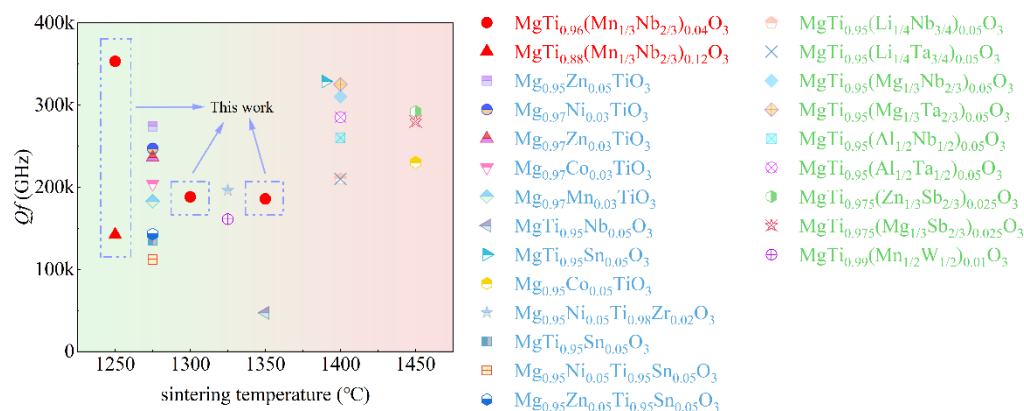


Figure 8. Comparison of Qf and sintering temperature relationship for MgTiO_3 -based ceramics in different literature.

4. Conclusions

The investigation of $\text{MgTi}_{1-x}(\text{Mn}_{1/3}\text{Nb}_{2/3})_x\text{O}_3$ ($x = 0-0.30$) ceramics revealed the presence of the MgTiO_3 phase, while MgTi_2O_5 was exclusively detected at $x = 0$ and $x = 0.30$. The observed variations in ϵ_r values demonstrated a correlation with the relative density and molecular polarization rate. The P-V-L theory supports the notion that higher lattice distortion leads to enhanced Qf values, which was evident at $x = 0.04$. Consequently, the substitution of Ti sites with $(\text{Mn}_{1/3}\text{Nb}_{2/3})^{4+}$ ions emerged as a promising strategy for improving the microwave dielectric properties of the ceramics. This substitution induced significant distortions in the TiO_6 octahedra, resulting in increased bond-restoring power. These structural modifications led to the emergence of τ_ϵ effects, ultimately manifested in τ_f values. Remarkably, the $x = 0.04$ $\text{MgTi}_{1-x}(\text{Mn}_{1/3}\text{Nb}_{2/3})_x\text{O}_3$ ceramics exhibited outstanding microwave dielectric properties when sintered at 1250°C , with $\epsilon_r = 17$, $Qf = 353,000$ GHz, and $\tau_f = -69$ ppm/ $^\circ\text{C}$. Consequently, these $\text{MgTi}_{1-x}(\text{Mn}_{1/3}\text{Nb}_{2/3})_x\text{O}_3$ ceramics hold substantial potential for applications in microwave communications. The findings presented in this paper also inspire novel research directions aimed at enhancing Qf values in future ceramic products.

Supplementary Materials: The following supporting information can be downloaded at: <https://www.mdpi.com/article/10.3390/cryst13071050/s1>, Figure S1: The SEM images of $\text{MgTi}_{1-x}(\text{Mn}_{1/3}\text{Nb}_{2/3})_x\text{O}_3$ ceramics: $x = 0$, 1250°C .

Author Contributions: Methodology, B.L. and F.W.; investigation, H.H. and F.W.; resources, Y.L.; data curation, B.L. and H.H.; writing—original draft preparation, B.L. and F.W.; writing—review and editing, H.H.; visualization, B.L.; supervision, Y.L. and G.J. All authors have read and agreed to the published version of the manuscript.

Funding: This research was funded by the Sichuan Science and Technology Program (No. 2023YFQ0082); Guangdong Provincial Key Laboratory of Electronic Functional Materials and Devices, grant number EFMD2022005Z; State Key Laboratory of Advanced Technologies for Comprehensive Utilization of Platinum Metals under Grant No. SKL-SPM-202021; Sichuan Province Science and Technology Department Key Research and Development Project, grant number 2022YFG0347.

Data Availability Statement: Data available on request from the corresponding author.

Acknowledgments: We extend our heartfelt appreciation to all the authors involved in this paper for their invaluable contributions to the work, as well as our sincere gratitude to the funders for their generous support.

Conflicts of Interest: The authors declare no conflict of interest.

References

1. Jo, H.J.; Kim, J.S.; Kim, E.S. Microwave dielectric properties of MgTiO₃-based ceramics. *Ceram. Int.* **2015**, *41*, S530–S536. [[CrossRef](#)]
2. Pullar, R.C.; Penn, S.J.; Wang, X.; Reaney, I.M.; Alford, N.M. Dielectric loss caused by oxygen vacancies in titania ceramics. *J. Eur. Ceram. Soc.* **2009**, *29*, 419–424. [[CrossRef](#)]
3. Gogoi, P.; Singh, L.R.; Pamu, D. Characterization of Zn doped MgTiO₃ ceramics: An approach for RF capacitor applications. *J. Mater. Sci. Mater. Electron.* **2017**, *28*, 11712–11721. [[CrossRef](#)]
4. Zhang, M.; Li, L.; Xia, W.; Liao, Q. Structure and properties analysis for MgTiO₃ and (Mg_{0.97}M_{0.03})TiO₃ (M=Ni, Zn, Co and Mn) microwave dielectric materials. *J. Alloys Compd.* **2012**, *537*, 76–79. [[CrossRef](#)]
5. Jia, X.; Xu, Y.; Zhao, P.; Li, J.; Li, W. Structural dependence of microwave dielectric properties in ilmenite-type Mg(Ti_{1-x}Nb_x)O₃ solid solutions by Rietveld refinement and Raman spectra. *Ceram. Int.* **2021**, *47*, 4820–4830. [[CrossRef](#)]
6. Gong, Z.; Wang, Z.; Wang, L.; Fu, Z.; Han, W.; Zhang, Q. Microwave dielectric properties of high-Q Mg(Sn_xTi_{1-x})O₃ ceramics. *Electron. Mater. Lett.* **2013**, *9*, 331–335. [[CrossRef](#)]
7. Manan, A.; Ullah, Z.; Ahmad, A.S.; Ullah, A.; Khan, D.F.; Hussain, A.; Khan, M.U. Phase microstructure evaluation and microwave dielectric properties of (1 - x)Mg_{0.95}Ni_{0.05}Ti_{0.98}Zr_{0.02}O_{3-x}Ca_{0.6}La_{0.8/3}TiO₃ ceramics. *J. Adv. Ceram.* **2018**, *7*, 72–78. [[CrossRef](#)]
8. Jo, H.J.; Kim, E.S. Enhanced quality factor of MgTiO₃ ceramics by isovalent Ti-site substitution. *Ceram. Int.* **2016**, *42*, 5479–5486. [[CrossRef](#)]
9. Fang, Z.; Yang, H.; Yang, H.; Xiong, Z.; Zhang, X.; Zhao, P.; Tang, B. Ilmenite-type MgTiO₃ ceramics by complex (Mn_{1/2}W_{1/2})⁴⁺ cation co-substitution producing improved microwave characteristics. *Ceram. Int.* **2021**, *47*, 21388–21397. [[CrossRef](#)]
10. Kim, J.M.; Jo, H.W.; Kim, E.S. Effect of electronegativity on microwave dielectric properties of MgTi_{1-x}(A_{1/3}Sb_{2/3})_xO₃ (A = Mg²⁺, Zn²⁺) ceramics. *Int. J. Appl. Ceram. Technol.* **2019**, *16*, 2053–2059. [[CrossRef](#)]
11. Jo, H.J.; Kim, E.S. Dependence of microwave dielectric properties on the complex substitution for Ti-site of MgTiO₃ ceramics. *Ceram. Int.* **2017**, *43*, S326–S333. [[CrossRef](#)]
12. Li, B.; Lai, Y.; Zeng, Y.; Yang, F.; Huang, F.; Yang, X.; Wang, F.; Wu, C.; Zhong, X.; Su, H. Structure and microwave dielectric properties of (Zn_{1/3}Nb_{2/3})⁴⁺ co-substituted MgTiO₃ ceramic. *Mater. Sci. Eng. B* **2022**, *276*, 115572. [[CrossRef](#)]
13. Yu, Y.; Guo, W.; Zhen, Y.; Cen, Z.; Ji, A.; Wu, H.; Liang, S.; Xiong, S.; Wang, X. Influence of MnO₂ addition on the dielectric properties of 0.95MgTiO₃-0.05CaTiO₃ ceramics sintered in a reducing atmosphere. *J. Eur. Ceram. Soc.* **2023**, *43*, 378–383. [[CrossRef](#)]
14. Rodríguez-Carvajal, J. Recent advances in magnetic structure determination by neutron powder diffraction. *Phys. B Phys. Condens. Matter* **1993**, *192*, 55–69. [[CrossRef](#)]
15. Shannon, R.D. Revised effective ionic radii and systematic studies of interatomic distances in halides and chalcogenides. *Acta Crystallogr. Sect. A* **1976**, *32*, 751–767. [[CrossRef](#)]
16. Xiao, M.; Wei, Y.; Gu, Q.; Zhang, P. The relationship between the bond ionicity, lattice energy, bond energy and microwave dielectric properties of LaNbO₄ ceramics. *J. Mater. Sci. Mater. Electron.* **2018**, *29*, 9963–9970. [[CrossRef](#)]
17. Zhang, Q.; Su, H.; Zhong, M.; Li, Y.; Tang, X.; Jing, Y. Bond characteristics and microwave dielectric properties on Zn_{3-x}Cu_x(BO₃)₂ ceramics with ultralow dielectric loss. *Ceram. Int.* **2021**, *47*, 4466–4474. [[CrossRef](#)]
18. Yao, G.-G.; Hou, C.-D.; Pei, C.-J.; Liu, P. Effects of Mg(OH)₂ on phase formation and microwave dielectric properties of Mg₆Ti₅O₁₆ ceramics. *Ferroelectrics* **2019**, *536*, 156–161. [[CrossRef](#)]
19. Chu, X.; Gan, L.; Ren, S.; Wang, J.; Ma, Z.; Jiang, J.; Zhang, T. Low-loss and temperature-stable (1 - x)Li₂TiO_{3-x}Li₃Mg₂NbO₆ microwave dielectric ceramics. *Ceram. Int.* **2020**, *46*, 8413–8419. [[CrossRef](#)]
20. Lou, W.C.; Song, K.X.; Hussain, F.; Liu, B.; Bafrooei, H.B.; Lin, H.X.; Su, W.T.; Shi, F.; Wang, D.W. Bond characteristics and microwave dielectric properties of (Li_{0.5}Ga_{0.5})²⁺ doped Mg₂Al₄Si₅O₁₈ ceramics. *Ceram. Int.* **2020**, *46*, 28631–28638. [[CrossRef](#)]
21. Forghani, M.; Paydar, M.H.; Podonak, M.K.; Li, L. Microstructure and dielectric properties of novel MgTiO_{3-x} wt% MgAl₂O₄ microwave dielectric composite ceramics. *J. Mater. Sci. Mater. Electron.* **2023**, *34*, 690. [[CrossRef](#)]
22. Liou, Y.-C.; Yang, S.-L. Calcium-doped MgTiO₃-MgTi₂O₅ ceramics prepared using a reaction-sintering process. *Mater. Sci. Eng. B* **2007**, *142*, 116–120. [[CrossRef](#)]
23. Yang, X.-Z.; Yang, F.; Lai, Y.-M.; Li, B.-Y.; Wang, F.-S.; Su, H. Effect of Cu²⁺ Ion A-Site Substitution on Structure and Dielectric Properties of MgTiO₃ Ceramics. *Chin. J. Inorg. Chem.* **2022**, *38*, 599–610. [[CrossRef](#)]
24. Fu, Z.; Chen, C.; She, Y.; Yang, Z.; Li, C. A/B Site Modified MgTiO₃ Dielectric Ceramics for Microwave Application. *Integr. Ferroelectr.* **2022**, *230*, 78–84. [[CrossRef](#)]
25. Sharma, K.; Bahel, S. Effect of Co substitution on the structural, dielectric and reflection properties of MgTiO₃ solid solutions. *Mater. Res. Bull.* **2023**, *157*, 112037. [[CrossRef](#)]
26. Xu, Z.; Li, L.; Yu, S.; Du, M.; Luo, W. Magnesium fluoride doped MgTiO₃ ceramics with ultra-high Q value at microwave frequencies. *J. Alloys Compd.* **2019**, *802*, 1–5. [[CrossRef](#)]

27. Rabha, S.; Dobbidi, P. Structural, electrical properties and stability in microwave dielectric properties of $(1 - x)$ MgTiO₃- x SrTiO₃ composite ceramics. *J. Alloys Compd.* **2021**, *872*, 159726. [[CrossRef](#)]
28. Singh, J.; Bahel, S. Synthesis of single phase MgTiO₃ and influence of Sn⁴⁺ substitution on its structural, dielectric and electrical properties. *J. Alloys Compd.* **2020**, *816*, 152679. [[CrossRef](#)]
29. Shi, L.; Peng, R.; Zhang, H.; Liu, C.; Gan, G.; Shi, X.; Wang, X. Effects of Magnesium–Tungsten co-substitution on crystal structure and microwave dielectric properties of CaTi_{1-x}(Mg_{1/2}W_{1/2})_xO₃ ceramics. *Ceram. Int.* **2021**, *47*, 3354–3360. [[CrossRef](#)]
30. Yang, H.; Zhang, S.; Li, Y.; Yang, H.; Yuan, Y.; Wen, T.; Li, E. Investigations of dielectric properties of wolframite A_{0.5}Zr_{0.5}NbO₄ ceramics by bond theory and far-infrared spectroscopy. *Ceram. Int.* **2020**, *46*, 3688–3694. [[CrossRef](#)]
31. Li, H.; Tang, B.; Li, X.; Qing, Z.; Li, Y.; Yang, H.; Wang, Q.; Zhang, S. The structure and properties of 0.95MgTiO₃-0.05CaTiO₃ ceramics doped with Co₂O₃. *J. Mater. Sci.* **2014**, *49*, 5850–5855. [[CrossRef](#)]
32. Liang, Z.; Li, J.; Zhang, Y.; Lu, B.; Han, X.; Yang, Y.; Zhang, H. Influence of CuO additive on phase formation, microstructure and microwave dielectric properties of Cu-doped Cu_xZn_{1.8-x}SiO_{3.8} ceramics. *Appl. Phys. A* **2021**, *128*, 1–8. [[CrossRef](#)]
33. Li, C.; Ding, S.; Zhang, Y.; Zhu, H.; Song, T. Effects of Ni²⁺ substitution on the crystal structure, bond valence, and microwave dielectric properties of BaAl₂-2Ni₂Si₂O₈ ceramics. *J. Eur. Ceram. Soc.* **2021**, *41*, 2610–2616. [[CrossRef](#)]
34. Bosman, A.J.; Havinga, E.E. Temperature Dependence of Dielectric Constants of Cubic Ionic Compounds. *Phys. Rev.* **1963**, *129*, 1593–1600. [[CrossRef](#)]
35. Sohn, J.-H.; Inaguma, Y.; Yoon, S.-O.; Itoh, M.; Nakamura, T.; Yoon, S.-J.; Kim, H.-J. Microwave Dielectric Characteristics of Ilmenite-Type Titanates with High Q Values. *Jpn. J. Appl. Phys.* **1994**, *33*, 5466–5470. [[CrossRef](#)]

Disclaimer/Publisher’s Note: The statements, opinions and data contained in all publications are solely those of the individual author(s) and contributor(s) and not of MDPI and/or the editor(s). MDPI and/or the editor(s) disclaim responsibility for any injury to people or property resulting from any ideas, methods, instructions or products referred to in the content.